The Astrophysical Journal, 702:1068–1077, 2009 September 10 doi:10.1088/0004-637X/702/2/1068

DEPENDENCE OF *s*-PROCESS NUCLEOSYNTHESIS IN MASSIVE STARS ON TRIPLE-ALPHA AND $^{12}C(\alpha, \gamma)^{16}O$ REACTION RATE UNCERTAINTIES

Clarisse Tur[1,5], Alexander Heger[2,3,4,5], and Sam M. Austin[1,5]
[1] National Superconducting Cyclotron Laboratory, Michigan State University, 1 Cyclotron Laboratory, East Lansing, MI 48824-1321, USA; tur@nscl.msu.edu, austin@nscl.msu.edu
[2] School of Physics and Astronomy, University of Minnesota, Twin Cities, Minneapolis, MN 55455-0149, USA
[3] Theoretical Astrophysics Group, MS B227, Los Alamos National Laboratory, Los Alamos, NM 87545, USA
[4] Department of Astronomy and Astrophysics, University of California, Santa Cruz, CA 95064, USA; alex@physics.umn.edu
Received 2008 September 1; accepted 2009 July 17; published 2009 August 18

ABSTRACT

We have studied the sensitivity of *s*-process nucleosynthesis in massive stars to $\pm 2\sigma$ variations in the rates of the triple-α and $^{12}C(\alpha, \gamma)^{16}O$ reactions. We simulated the evolution of massive stars from H burning through Fe-core collapse, followed by a supernova explosion. We found that the production factors of *s*-process nuclides between ^{58}Fe and ^{96}Zr change strongly with changes in the He burning reaction rates; using the Lodders solar abundances rather than those of Anders and Grevesse reduces *s*-process nucleosynthesis; later burning phases beyond core He burning and shell C burning have a significant effect on post-explosive production factors. We also discuss the implications of the uncertainties in the helium burning rates for evidence of a new primary neutron capture process (LEPP) in massive stars.

Key words: nuclear reactions, nucleosynthesis, abundances – supernovae: general

Online-only material: color figures

1. INTRODUCTION

Half of the elements between Fe and Bi are produced by the slow (*s*) neutron capture process and most of the remainder by the rapid (*r*) neutron capture process. About 35 additional neutron deficient stable nuclides above ^{56}Fe, the *p*-process nuclei, are produced in explosive processes (Prantzos et al. 1990b).

Two components, the main and the weak *s*-processes, are required to explain the isotopic distributions of *s*-process nuclides. The main *s*-process occurs in low-mass ($\lesssim 4\,M_\odot$) asymptotic giant branch (AGB) stars and contributes mainly to the production of heavier elements, with a smaller contribution to $A \leqslant 90$. The weak *s*-process occurs during the late evolutionary stages of massive stars ($\gtrsim 10\,M_\odot$) and produces nuclides up to $A \simeq 90$.

Recently, Travaglio et al. (2004) summed the contributions of the *r*-process, the main and weak *s*-processes, and the *p*-process to the abundances of Sr, Y, and Zr. The summed contributions were smaller than the observed solar abundances by 8%, 18%, and 18%, respectively. They concluded that an additional light element primary *s*-process (LEPP) contribution from massive stars is needed to explain this difference; the nature and site of the LEPP are unknown. This LEPP has also been invoked by Montes et al. (2007) to explain the abundances of a larger group of light *r*-process elements. Since the LEPP effects are relatively small, and since some of the LEPP elements are produced with relatively large abundance in the weak *s*-process, it is important to establish whether the uncertainties in the weak *s*-process are sufficiently small that the claim of LEPP contributions is robust.

Nuclide production in the weak *s*-process also depends on the rate of the neutron source $^{22}Ne(\alpha, n)^{25}Mg$ and on the capture cross sections for the neutron poisons (medium-weight isotopes up to Fe, including ^{12}C, ^{16}O, ^{20}Ne, ^{22}Ne, ^{23}Na, ^{24}Mg, and ^{25}Mg). Neither the source strength nor the neutron capture cross sections for the poisons are known with sufficient accuracy (Heil et al. 2008). We shall not deal with these issues in this paper, but rather with the more indirect effects of uncertainties in the rates ($R_{3\alpha}$ and $R_{\alpha,12}$) of the triple alpha and $^{12}C(\alpha, \gamma)^{16}O$ reactions, and in the initial stellar composition. For example, we have shown in a previous paper (Tur et al. 2007; see also Weaver & Woosley 1993; Woosley et al. 2003; Woosley & Heger 2007), that the amount of the above neutron poisons present during the weak *s*-process in massive stars depends sensitively on these rates and the initial stellar composition.

Most earlier studies of the weak *s*-process focused on production toward the end of core He burning by neutrons from the $^{22}Ne(\alpha, n)^{25}Mg$ reaction (Couch et al. 1974; Lamb et al. 1977; Arnett et al. 1985; Busso & Gallino 1985; Langer et al. 1989; Prantzos et al. 1990a; The et al. 2000; Raiteri et al. 1991b; Baraffe et al. 1992). Later papers considered also a second exposure at higher temperatures and neutron densities peaking during shell C burning (Raiteri et al. 1991a, 1992, 1993; The et al. 2007). Explosive processing in the supernova explosion was not considered. Recent calculations of *s*-process yields have been extended to consider the entire evolutionary history of the star, including explosive burning (Hoffman et al. 2001; Rauscher et al. 2002; Limongi & Chieffi 2003).

In this paper, we simulate the evolution of massive stars from H burning through Fe-core collapse, followed by a supernova explosion. Our principal purposes are (1) to establish the magnitude of weak *s*-process production in a self-consistent model; (2) to study the uncertainties in weak *s*-process nucleosynthesis arising from uncertainties in $R_{3\alpha}$ and $R_{\alpha,12}$; (3) to study the effects of different stellar abundances, specifically those of Lodders (2003) and Anders & Grevesse (1989), hereafter L03 and AG89; (4) to delineate the stages of stellar evolution during which weak *s*-process elements are produced; and (5) to assess the bearing of these uncertainties on the robustness of the LEPP process.

[5] Joint Institute for Nuclear Astrophysics, Michigan State University, East Lansing, MI 44824, USA.

In Section 2, we describe the stellar model and the input physics relevant to the treatment of the weak *s*-process. Section 3 gives our results for the dependence of the post-explosive weak *s*-process production factors on changes in the rates of the helium burning reactions and on different initial stellar abundances. In Section 4, we show the contribution to the weak *s*-process abundances of the various stellar burning stages prior to the supernova explosion. In Section 5, we investigate the range of weak *s*-process production of Sr, Y, and Zr allowed by the uncertainties in the helium burning reactions.

2. STELLAR MODELS AND INPUT PHYSICS

The one-dimensional hydrodynamics code KEPLER (Weaver et al. 1978; Woosley & Weaver 1995; Rauscher et al. 2002; Woosley et al. 2002) is used to evolve stars from central H burning up to Fe-core collapse. The supernova explosion that follows is simulated using a spherical piston placed at the base of the O burning shell, which first moves inward and then outward at a constant acceleration which has been adjusted to result in a total kinetic energy of the ejecta of 1.2×10^{51} erg one year after the explosion, and coming to rest at a radius of 1000 km (Rauscher et al. 2002; Woosley & Heger 2007). After estimating the fallback from our hydrodynamic supernova simulations, the final nucleosynthesis yields are determined by employing the same parameterization of mixing as was used by Woosley & Heger (2007).

We performed calculations for stars of 15, 20, and 25 $M_\odot$ and for two different initial abundances, L03 and AG89. Rate sets were: (1) $R_{3\alpha}$ was kept constant (at its value from Caughlan & Fowler 1988), and $R_{\alpha,12}$ was varied; (2) both rates were varied by the same factor, so their ratio remained constant; and (3) $R_{\alpha,12}$ was held constant at 1.2 times the rate recommended by Buchmann (1996) and $R_{3\alpha}$ was varied. Both reaction rates were varied within a range of $\pm 2\sigma$ of their experimental uncertainties.

For more details see Tur et al. (2007), Woosley & Heger (2007), and Rauscher et al. (2002) who give a complete description of the improvements to the stellar physics and reaction rates since Woosley & Weaver (1995). In particular, the "rath" rates, Rauscher & Thielemann (2000), have been adopted for the competing reactions ^{22}Ne$(\alpha, n)^{25}$Mg and ^{22}Ne$(\alpha, \gamma)^{26}$Mg.

We adopt a two-character notation to label our plots, e.g., LA, similar to the notation adopted by Tur et al. (2007). The first character can be an L (to denote the L03 initial abundances) or an A (for the AG89 initial abundances). The second character denotes the study: A, when $R_{3\alpha}$ was kept constant, and $R_{\alpha,12}$ was varied, B, when both rates were varied by the same factor, so their ratio remained constant, and C, when $R_{\alpha,12}$ was held constant, and $R_{3\alpha}$ was varied.

3. POST-EXPLOSIVE PRODUCTION FACTORS

In Figure 1, we show the evolution of the production factors as a function of $R_{\alpha,12}$ for isotopes between ^{58}Fe and ^{96}Zr. To facilitate reading, Figure 2 shows the same for the six *s*-only isotopes. We define the production factor for each stable isotope as the ratio of the mass fraction of the isotope in the supernova ejecta to its initial solar mass fraction. $R_{3\alpha}$ was kept constant at the value from Caughlan & Fowler (1988). The color bar range is from 1 to 3×10^2. The range of production factors for a 25 $M_\odot$ star is shown in Table 1. For most assumed reaction rates, production factors (PFs) obtained using the L03 abundances (Figures 1(b), (d), and (f)), are significantly smaller than those for the AG89 abundances (Figures 1(a), (c), and (e)). Presumably the lower CNO content of the L03 abundance set leads to a smaller amount of ^{22}Ne, lower neutron abundance, and a less efficient *s*-process (Woosley & Heger 2007).

We have shown in Tur et al. (2007) that for the range of reaction rates we calculate, the PF for ^{16}O is 10.0 ± 0.5 for the AG89 abundances, and 15.3 ± 0.5 for the L03 abundances; the uncertainty is the standard deviation of the results for the different rates. We find that the PFs we obtain for the *s*-process elements are often larger than this, see Figure 1 and Table 1. This is not surprising: very low metallicity stars produce oxygen, but very small abundances of the secondary weak *s*-process nuclei. We next use a simple model to estimate what PF in a solar-abundance star would be required to reproduce the observed abundances.

Assume that a nuclide X is to be produced entirely by secondary processes in massive stars. It follows that when integrated over metallicities from zero to the present, its PF must be the same as that for ^{16}O. Solar-metallicity stars must, therefore, have a larger PF for X than for ^{16}O. In a simple closed-box model, assuming the production of X is proportional to metallicity, the required ratio of secondary to primary production in a solar-abundance star is two. We take this as a working hypothesis, bearing in mind that it is only a rough approximation. Then, if the PF for a weak-*s* nuclide is $2\times$PF(^{16}O), massive stars produce the observed solar abundance, or if it is equal to PF(^{16}O), half the observed abundance. The fraction f of the observed solar abundance for nuclide X produced in our model is given by

$$f(X) = 0.5 \times \mathrm{PF}(X)/\mathrm{PF}(^{16}\mathrm{O}), \quad (1)$$

where the 0.5 arises from the model described above; as noted above PF(^{16}O) is approximately 10 (15.3) for the AG89 (L03) abundances. Equation (1) and Figure 1 can be used to estimate whether a particular isotope is overproduced for a given star or rate choice.

The production factors increase strongly as the stellar mass increases, reflecting a more efficient *s*-process as the temperature increases. In particular, most isotopes are weakly produced, PF < 20 (30) for AG89 (L03) in the 15 $M_\odot$ star, with the exception of those between ^{58}Fe and ^{65}Cu, and of some isotopes when $R_{\alpha,12}$ is given its lowest or highest value (Figures 1(a) and (b)). The highest PFs are observed for the 25 $M_\odot$ star (Figures 1(e) and (f)), whereas the 20 $M_\odot$ star shows a contribution between those two extremes (Figures 1(c) and (d)). Ignoring the contribution of the 15 $M_\odot$ and 20 $M_\odot$ stars as was done in Raiteri et al. (1991b) and Raiteri et al. (1991a) does not seem justified; their contributions are not always negligible.

We find that ^{62}Ni is overproduced for many rate choices, especially for the 25 $M_\odot$ star and the AG89 abundances. This problem was already documented by Rauscher et al. (2002) and seems to arise from the decreased value of the ^{62}Ni$(n, \gamma)^{63}$Ni reaction rate used for our models compared to its previous compilation. The factor of 3 change arises from different extrapolations of a cross section measured only at thermal neutron energies (see also Nassar et al. 2005, however).

Table 1 shows, for a 25 $M_\odot$ star of L03 initial abundance, the value of the maximum and minimum production factors for nuclides between ^{58}Fe and ^{96}Zr when either $R_{\alpha,12}$ or $R_{3\alpha}$ is varied within its $\pm 2\sigma$ uncertainties. Large differences in PFs are found when either $R_{3\alpha}$ or $R_{\alpha,12}$ are varied. Most commonly, the largest PFs are obtained for the lower values of $R_{\alpha,12}$ as one sees in Figure 1. Figure 3 shows some of the changes resulting

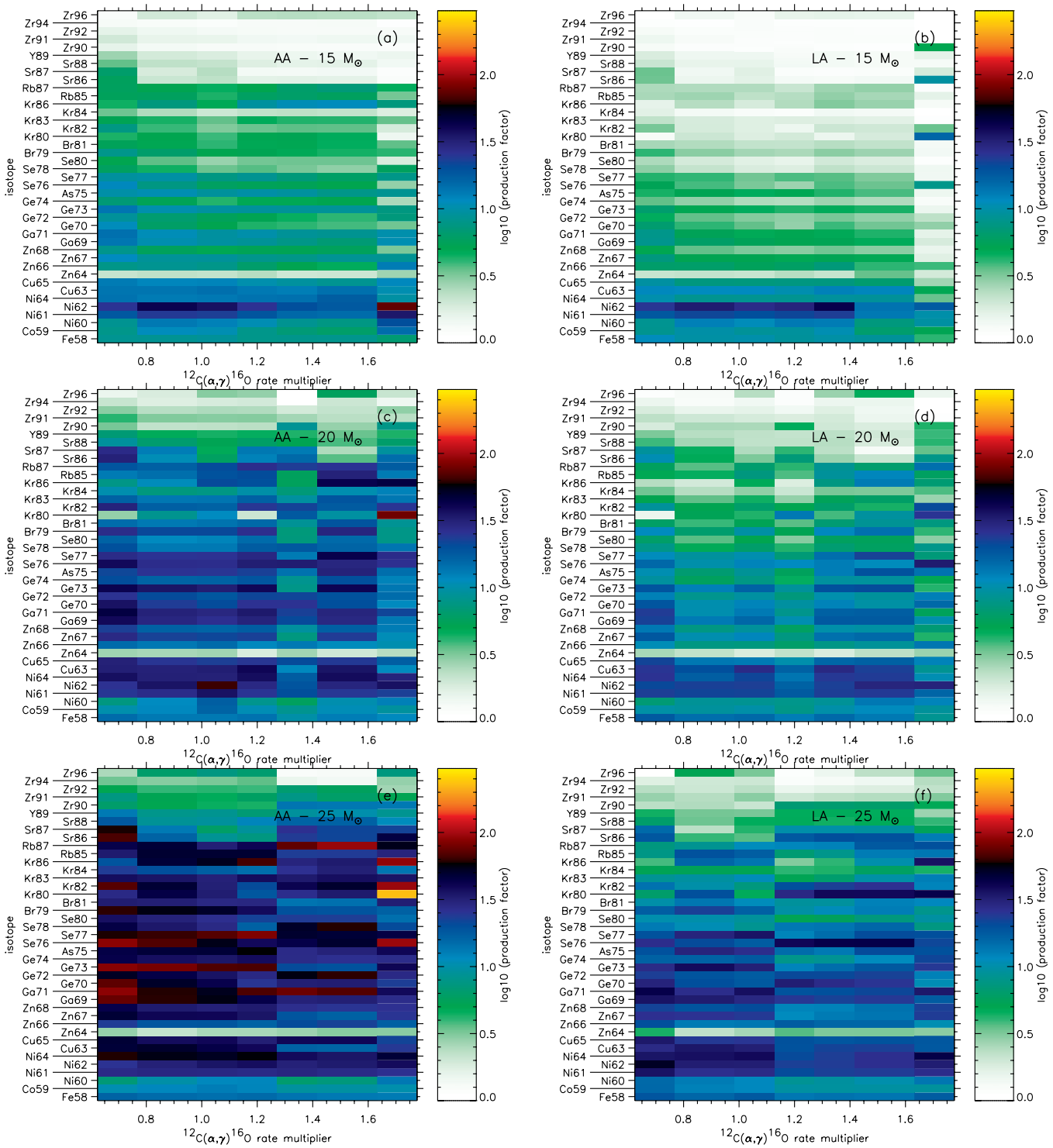

Figure 1. Post-explosive production factors as a function of $R_{\alpha,12}$. (a) The AA series, 15 $M_\odot$. (b) The LA series, 15 $M_\odot$. (c) The AA series, 20 $M_\odot$. (d) The LA series, 20 $M_\odot$. (e) The AA series, 25 $M_\odot$. (f) The LA series, 25 $M_\odot$.

from changes in $R_{3\alpha}$. Lower values of $R_{3\alpha}$ lead to lower ^{12}C abundance at the end of central helium burning. This, in turn, is compensated by a slightly higher central temperature to produce the same energy release rate to maintain the star's luminosity. Due to the high temperature sensitivity of the ^{22}Ne(α, n) reaction this increased temperature means more of the ^{22}Ne has been burnt by central helium depletion, resulting in a stronger *s*-process. Figure 3 also shows the decrease of ^{56}Fe for lower $R_{3\alpha}$ that correlates very well with the smaller amount of ^{22}Ne left, i.e., more of it being burnt, providing a measure of neutron exposure.

For many isotopes, the maximum PF is greater than twice the minimum. For example, for $\pm 2\sigma$ uncertainties in $R_{\alpha,12}$ the PF for ^{73}Ge ranges from 1.5 to 6.5; 4.2 to 20.9; 12.1 to 38.0 for 15 $M_\odot$; 20 $M_\odot$; 25 $M_\odot$ stars, respectively. The *s*-only isotopes show a similarly strong sensitivity. For $\pm 2\sigma$ uncertainties in $R_{\alpha,12}$, the PF for ^{70}Ge, an *s*-only isotope, decreases from 6.6 to 2.2; 18.8 to 9.5; 32.5 to 10.9 for 15 $M_\odot$;

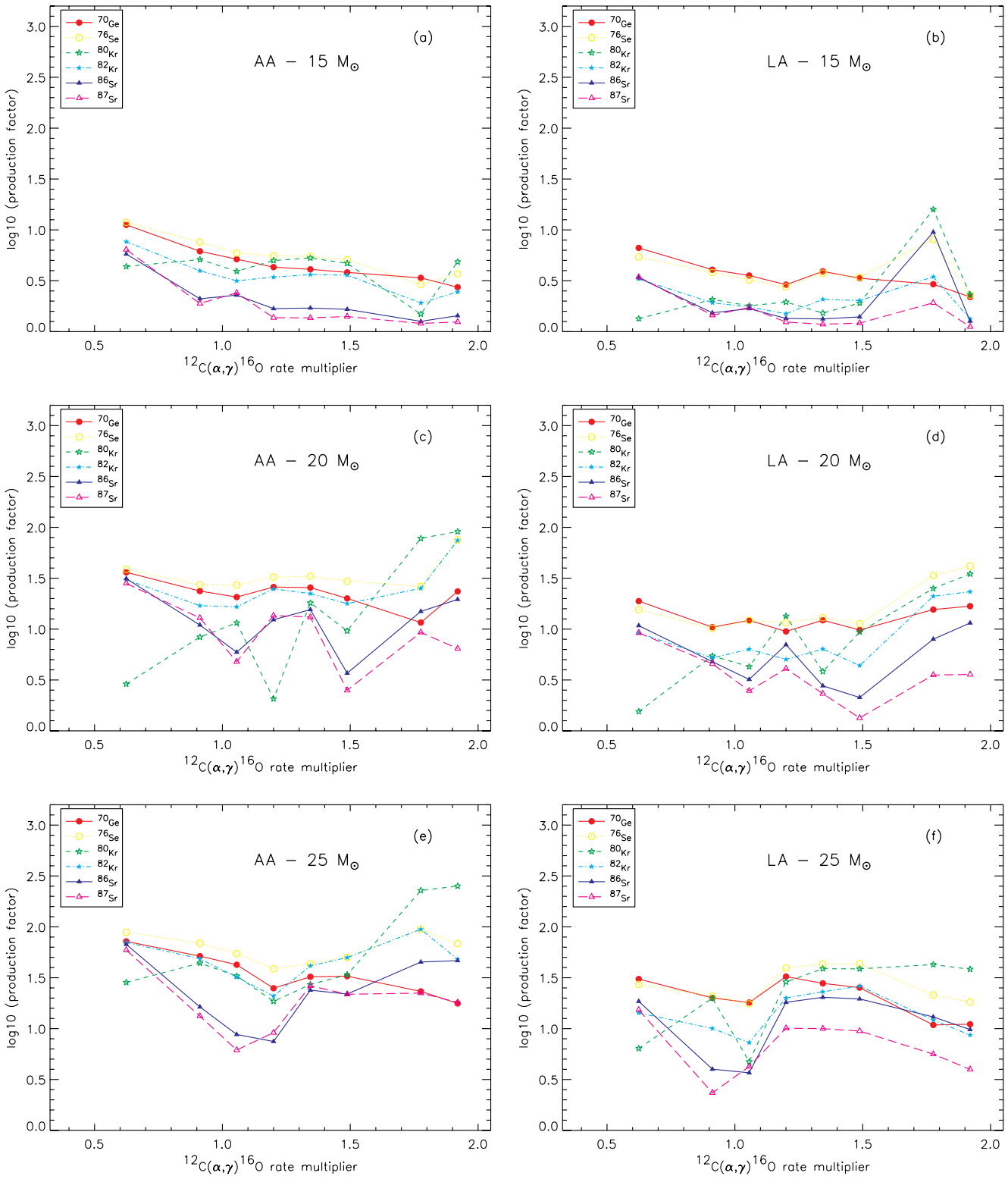

Figure 2. Post-explosive production factors for *s*-only isotopes as a function of $R_{\alpha,12}$. (a) The AA series, 15 $M_{\odot}$. (b) The LA series, 15 $M_{\odot}$. (c) The AA series, 20 $M_{\odot}$. (d) The LA series, 20 $M_{\odot}$. (e) The AA series, 25 $M_{\odot}$. (f) The LA series, 25 $M_{\odot}$.

(A color version of this figure is available in the online journal.)

20 $M_{\odot}$; 25 $M_{\odot}$ stars. For an average over the three stars, the production factor for ^{80}Kr, another *s*-only isotope, ranges from 2.5 at the lowest value of $R_{\alpha,12}$ to 20.5 at its next to highest value.

In Figure 4, we illustrate the variations in the production factors for a 25 $M_{\odot}$ star with the L03 initial abundances when $R_{3\alpha}$ is varied and $R_{\alpha,12}$ is held constant (Figure 4(a)), and when both reaction rates are varied by the same amount (Figure 4(b)). To facilitate reading, we show the same for the six *s*-only isotopes in Figure 5. Large variations in the production factors are observed in both cases, demonstrating the importance of both helium burning reactions.

Table 1
Minimum and Maximum Values of the *s*-Process Production Factors for a 25 $M_\odot$ Star with L03 Initial Abundances

Isotope	Within 2σ Errors in $R_{\alpha,12}$		Within 2σ Errors in $R_{3\alpha}$	
	Maximum	Minimum	Maximum	Minimum
^{58}Fe	18.8	13.7	19.1	13.1
^{59}Co	15.6	9.3	12.0	9.2
^{60}Ni	16.2	8.7	11.9	6.0
^{61}Ni	36.1	20.7	29.6	20.7
^{62}Ni	52.5	22.8	31.3	22.8
^{64}Ni	43.8	21.0	37.7	21.0
^{63}Cu	35.0	14.1	33.2	14.3
^{65}Cu	34.5	18.5	26.5	19.7
^{64}Zn	4.4	2.3	3.7	2.2
^{66}Zn	19.9	10.8	20.0	10.5
^{67}Zn	26.3	11.4	22.9	11.4
^{68}Zn	22.8	12.2	20.0	12.2
^{69}Ga	36.0	17.3	32.6	21.8
^{71}Ga	43.8	19.2	40.7	19.2
^{70}Ge	32.5	10.9	36.3	13.8
^{72}Ge	23.2	12.4	28.7	11.9
^{73}Ge	38.0	12.1	30.2	11.7
^{74}Ge	25.1	8.0	16.8	8.0
^{75}As	30.4	13.4	30.2	12.9
^{76}Se	43.5	17.5	54.3	13.9
^{77}Se	35.8	12.2	30.3	12.2
^{78}Se	15.6	7.6	20.0	6.4
^{80}Se	13.3	5.3	10.4	5.3
^{79}Br	22.7	7.2	17.8	9.3
^{81}Br	13.8	8.3	16.7	6.7
^{80}Kr	42.6	4.7	47.6	4.1
^{82}Kr	26.2	7.3	29.9	5.5
^{83}Kr	12.7	5.3	12.6	5.3
^{84}Kr	6.0	4.1	6.6	3.8
^{86}Kr	48.4	3.1	13.1	3.1
^{85}Rb	19.5	6.8	16.9	6.8
^{87}Rb	20.5	7.4	18.8	6.4
^{86}Sr	20.3	3.7	23.9	2.9
^{87}Sr	15.3	2.3	13.1	2.9
^{88}Sr	6.4	3.4	5.8	3.3
^{89}Y	4.7	2.6	5.8	2.8
^{90}Zr	6.8	2.1	8.0	1.9
^{91}Zr	3.1	1.6	3.9	2.1
^{92}Zr	3.1	1.5	3.2	1.5
^{94}Zr	2.4	1.2	2.0	1.2
^{96}Zr	5.3	1.0	3.3	1.0

The results shown in Figures 1 and 4 are consistent with the findings of Tur et al. (2007) that both reactions sensitively influence the production factors of the medium-weight isotopes, among which are the neutron poisons mentioned earlier. When, however, we examine the production of these poisons and of the weak-*s* isotopes, as a function of the rates, we find only weak indications of any correlation.

In Table 2, we compare our results for the *s*-only elements, using the central values of the reaction rates, with results of earlier calculations. The temperature dependence of the ^{79}Se beta decay rate is not implemented in KEPLER; this may account for the lower value of the production factor for ^{80}Kr compared to the result of The et al. (2007). Our values of weak-*s* production percentage are significantly larger than those of Raiteri et al. (1993) and The et al. (2007) presumably because of contributions from burning beyond O depletion. The present results have the correct trend, being smaller when the main

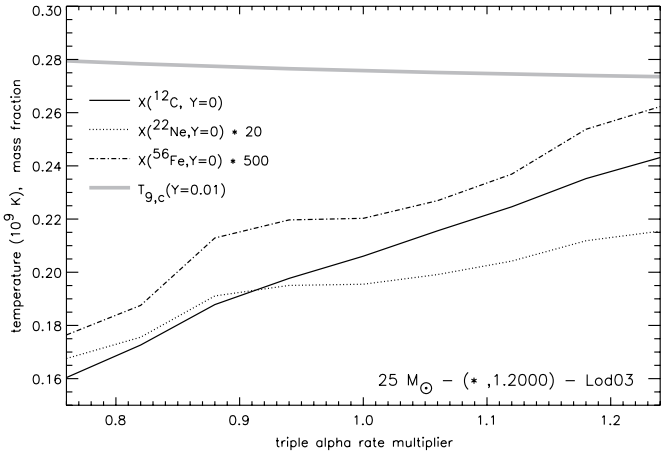

Figure 3. Central temperature at the end of central helium burning (1% helium mass fraction: "$Y = 0.01$") in units of 10^9 K ($T_{9,c}$), central abundances of ^{12}C, ^{22}Ne, and ^{56}Fe after core helium depletion ("$Y = 0.00$") for 25 $M_\odot$ stars with L03 initial abundance as a function of $R_{3\alpha}$.

s-process is large. Overall, however, the results for these central values of the rates are surprisingly large. But they are also very sensitive to the reaction rates. For example, for the L03 abundances, a 15% smaller value of the ^{12}C$(\alpha, \gamma)^{16}$O rate gives weak-*s* contributions at least a factor of 2 smaller for these nuclei. On the other hand, for the AG89 rates, the weak-*s* contributions would be still larger. This is yet another example of the sensitivity of supernova nucleosynthesis to the rates of the helium burning reactions, and further evidence of the need for more accurate rates.

4. EVOLUTION OF PRODUCTION FACTORS ALONG THE STELLAR BURNING HISTORY

In this section, we compare the contribution of various stellar burning phases to the *s*-process abundances for the 25 $M_\odot$ star, L03 initial abundances, and the central values of the helium burning reaction rates: $R_{3\alpha}$ from Caughlan & Fowler (1988), and $R_{\alpha,12}$ equal to 1.2 times the rate recommended by Buchmann (1996). Dump files are generated at specified times during the life of the star as shown in Figure 6. From these we extract the PFs for isotopes between ^{58}Fe and ^{96}Zr and plot them in Figure 7 versus their distance from the stellar center in solar masses. The PF is defined as the mass fraction of an isotope in a given stellar zone (or mass location) divided by its solar mass fraction. All the color bars of Figures 7(a)–(h) have the same scale (from 1 to 4×10^3) to facilitate comparison among them. Figures 7(a)–(g) show the evolution of production factors at various burning phases of the star, up to the pre-supernova stage. The black vertical line on the figures shows the location of the initial mass cut (i.e., the position of the piston at the base of the O burning shell right before the explosion). Only the stellar mass shells above that line have a chance of being ejected during the explosion. The gray shaded areas on Figures 7(f) and (g) show those regions of the star where nucleosynthesis calculations are no longer being performed because a nuclear statistical equilibrium network is employed and these layers are known to become a part of the iron core and will not mix with the layers above before core collapse. They also lie inside the piston, i.e., below the pre-supernova mass cut.

Below we give a detailed explanation for Figure 7:

1. Figure 7(a): at He ignition. Since no *s*-processing has yet occurred at this stage, the production factors are essentially zero.

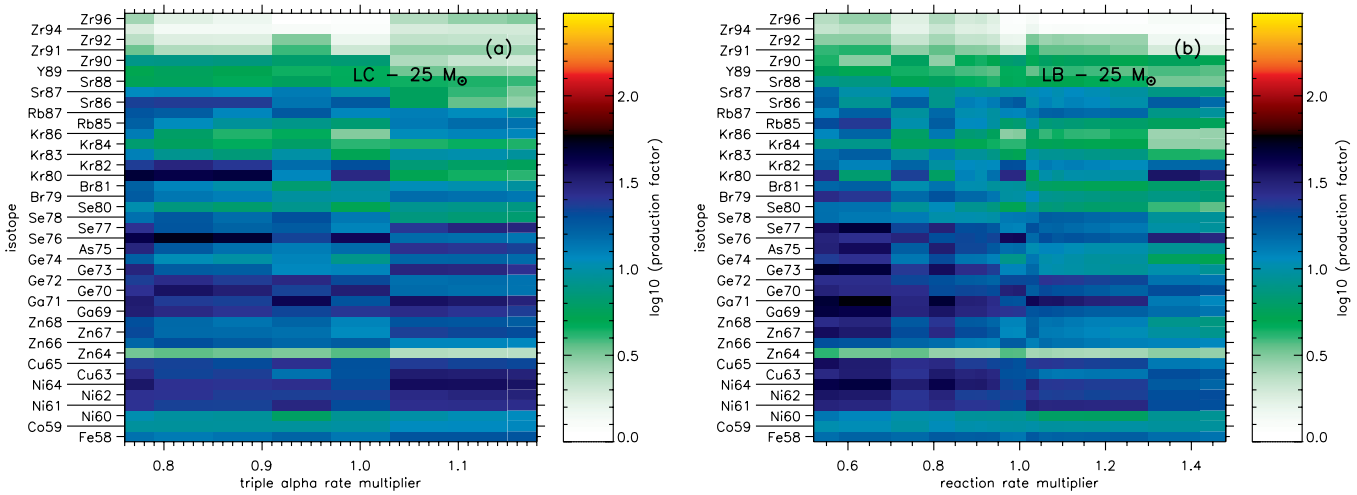

Figure 4. Post-explosive production factors for a 25 $M_{\odot}$ star as a function of $R_{3\alpha}$. (a) The LC series. (b) The LB series. The "reaction rate multiplier" is the factor that multiplies both the standard rates.

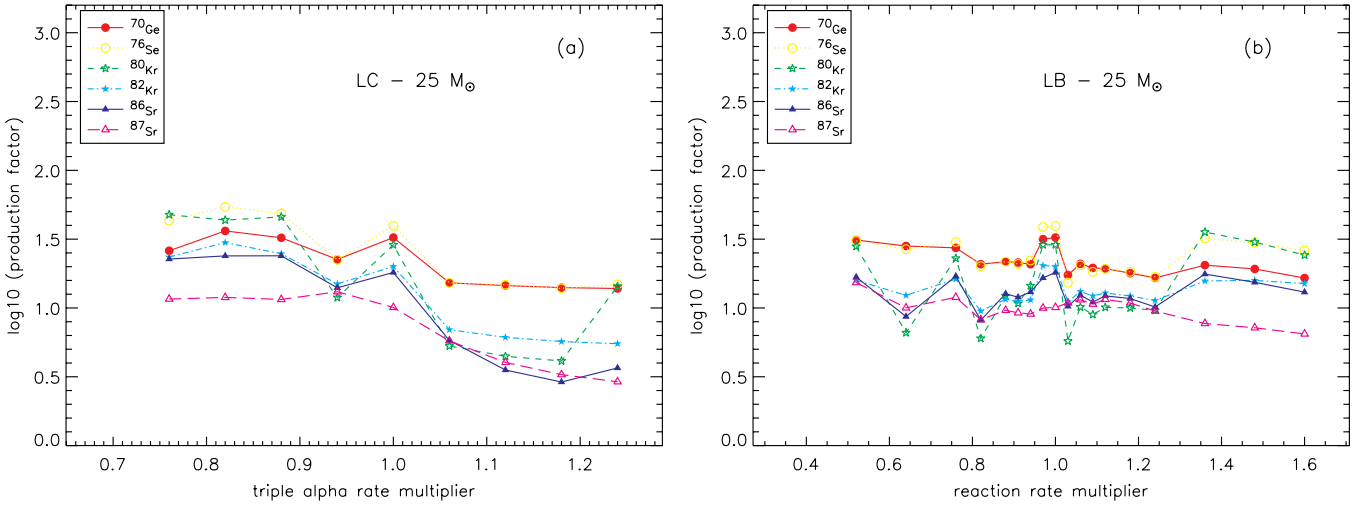

Figure 5. Post-explosive production factors for *s*-only isotopes for a 25 $M_{\odot}$ star as a function of $R_{3\alpha}$. (a) The LC series. (b) The LB series. The "reaction rate multiplier" is the factor that multiplies both the standard rates.

2. Figure 7(b): just before central He depletion (when the central He mass fraction has reached 1%). Central helium *s*-processing is in progress during this late He burning phase, as the temperatures become high enough to ignite ^{22}Ne$(\alpha, n)^{25}$Mg.

3. Figure 7(c): just before central C ignition (when the central temperature reaches a value of 5×10^8 K). Central helium burning has finished; this figure shows the final abundance and distribution of isotopes due to central helium burning. About 1/3 of this *s*-process yield is located inside the later mass cut (compact remnant) of the supernova. This has

Table 2
Percentage of *s*-only Nuclei Produced by the Weak *s*-Process for a 25 $M_{\odot}$ Star

Isotope	PF(X) AG	PF(X) The[a]	PF(X) Lod	PF(AG)/PF(Lod)	PF(X)/PF(^{16}O)AG	PF(X)/PF(^{16}O)Lod	%Weak-s AG[b]	%Weak-s Lod[b]	%Weak-s Raiteri[c]
^{70}Ge	24.9	32.9	32.5	0.8	2.49	2.12	124.7	106	64
^{76}Se	38.7	29.2	39.4	1.0	3.87	2.58	193.6	129	63
^{80}Kr	18.5	47.7	28.8	0.6	1.85	1.88	92.7	94	86
^{82}Kr	20.9	28.4	20.0	1.0	2.09	1.31	104.5	65	53
^{86}Sr	7.5	19.9	18.1	0.4	0.75	1.18	37.4	59	24
^{87}Sr	9.1	15.8	10.1	0.9	0.91	0.66	45.7	33	16

Notes.
[a] From The et al. (2007), results labeled 25 K in Table 7.
[b] Calculated using Equation (1).
[c] From Raiteri et al. (1993), Table 5.

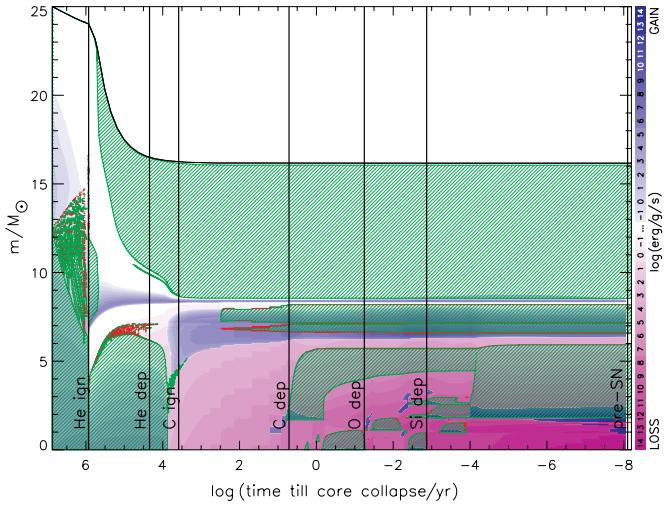

Figure 6. Energy history of the 25 $M_\odot$ star (central values of the reaction rates, L03 abundances) as a function of time until core collapse. The ordinate is the included mass from the stellar center. The green cross hatched areas are fully convective, and the red crosshatched areas are semiconvective. The blue and pink shading indicate net energy generation, with blue positive and pink negative. For more details, see Woosley et al. (2002). The vertical lines show the times when dump files are generated by the KEPLER code at key stages of the evolutionary process.

been largely neglected in most of the previous papers on the subject as it is hard to assess without simulation of the supernova.

4. Figure 7(d): central C depletion (when the central temperature has reached 1.2×10^9 K). Central C burning contributes mostly to those regions of the star below the mass cut. We also see the result of onset of the first carbon burning shell and of He shell burning (between mass coordinate of 6 $M_\odot$ and 7 $M_\odot$) which appears to be significant for most isotopes.
5. Figure 7(e): at central O depletion (when the central O mass fraction has dropped below 5%). Significant *s*-processing occurs during the C shell burning as seen in the enhancements to the PFs in the mass region above the mass cut. There is also photodissociation during central O burning in the region below the mass cut.
6. Figure 7(f): at Si depletion (when the central Si mass fraction drops below 10^{-4}). Additional photodissociation occurs during core Si burning. Very strong overproduction occurs for some isotopes close to the mass cut.
7. Figure 7(g): at the pre-supernova stage (when the contraction speed in the iron core reaches 1000 km s^{-1}).
8. Figure 7(h): 100 s after the passage of the shock wave. This panel shows the PFs above the mass cut, when most nuclear reactions cease due to the very low temperatures. The isotopes closest to the mass cut have essentially been destroyed with the exception of some local overproduction for isotopes below ^{70}Ge. These local enhancements can still lead to overall increased supernova yields after mixing and fallback.

In Figures 8(a)–(d), we show the production factors of single isotopes (^{70}Ge, ^{75}As, ^{80}Kr, and ^{87}Rb) for a 25 $M_\odot$ star versus the mass coordinate (1.2–3.5 $M_\odot$) at various times during the star's life, using the central values of the helium burning reaction rates. Figure 8(c) highlights the importance of the late evolutionary stages: most of the ^{80}Kr made during the stages up to pre-supernova is destroyed and rebuilt during the supernova explosion. For ^{70}Ge, ^{75}As, and ^{87}Rb, the C shell burning and the pre-supernova stages both have significant contributions for masses beyond about 2.5 $M_\odot$. The temperature dependence of the ^{79}Se beta decay rate is not implemented in KEPLER; the low values of the production factor for ^{80}Kr in the earlier evolutionary stages presumably reflect this fact. This comment also applies to Figure 9. The lower values of the ^{22}Ne(α, n)^{25}Mg rates used here may also contribute to smaller yields compared to some previous studies.

To assess the importance of various stages, we have determined the PFs for isotopes produced outside the mass cut at the times shown in Figure 6. It is clear from Figure 9 that the later evolutionary stages contribute significantly, especially for ^{80}Kr. In the cases of ^{86,87}Sr, however, little changes after oxygen depletion.

5. Sr, Y, Zr, AND THE LEPP PROCESS

As noted in the introduction, the LEPP process was introduced by Travaglio et al. (2004) to explain the excess of the observed abundances of some elements, especially Sr, Y, and Zr, above that produced by the *r*-process, the main and weak *s*-processes, and the *p*-process. We examine here the uncertainties in the weak *s*-process production of these elements. The differences shown in Table 1 and Figure 1 for individual isotopes appear much larger than the 8%–18% differences that led to the proposal of the LEPP process. These differences, however, are important only if, (1) the weak *s*-process makes a sufficient fraction of an isotope, and if, (2) the differences persist for the elemental differences, the observed quantities, not just the differences in a single isotope. We have calculated the elemental production factors for the 25 $M_\odot$ star and the integrated result for the 15 $M_\odot$, 20 $M_\odot$, and 25 $M_\odot$ stars, using the nominal reaction rates for $R_{3\alpha}$ and $R_{\alpha,12}$ and the L03 abundances. The results were averaged over an initial mass function (IMF) with a slope of $\gamma = -2.6$ (Scalo 1986) and divided by their solar mass fraction, as described in Tur et al. (2007). We summarize the relevant quantities in Table 3. For the 25 $M_\odot$ star taken alone, the uncertainties are significant, 10%–16% compared to the 8%–18% differences that were to be explained by the LEPP process. When one takes the averages over the 15 $M_\odot$, 20 $M_\odot$, and 25 $M_\odot$ stars, however, uncertainties are smaller, 3%–7%, but those for Sr are similar to the 8% LEPP effect. All of these uncertainties are upper limits, in the context of the present calculations, since they are the extreme values for the entire set of reaction rates. Differences in PFs for these elements tend to cancel when one adds the production for the three stars, but it is not known whether such cancellations will occur for other elements. And one must still consider the uncertainties arising from uncertainties in the rates of the neutron producing cross sections and the capture cross sections for various poisons as described in the introduction. Taken together, these considerations leave the LEPP process only moderately robust.

6. CONCLUSIONS

We followed the entire nucleosynthesis throughout the life of massive stars, from H burning through Fe-core collapse, followed by a supernova explosion. We observe a strong sensitivity of the PFs for weak *s*-process isotopes to $\pm 2\sigma$ variations of the rates of the triple-α and of the ^{12}C(α, γ)^{16}O reactions. This can be explained by the variations in the PFs of medium-weight neutron poisons found by Tur et al. (2007),

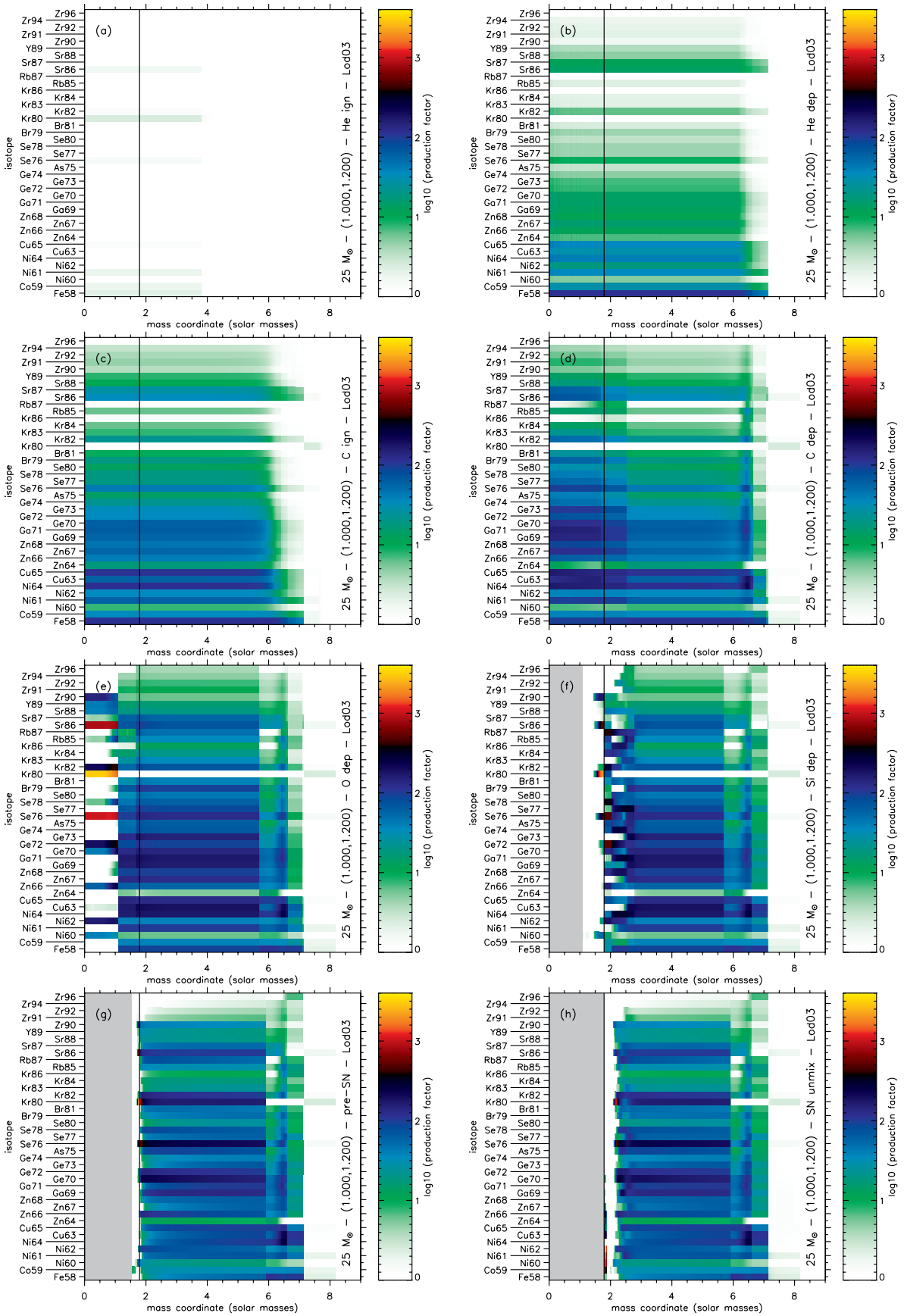

Figure 7. Production factors for *s*-process isotopes for a 25 $M_{\odot}$ star (L03 initial abundances) as a function of their mass location within the star. (a) At He ignition. (b) At central He depletion (1% He left). (c) After central He depletion but before central C ignition. (d) At central C depletion. (e) At central O depletion. (f) At central Si depletion. (g) At onset of core collapse. (h) 100 s after core collapse (after explosive nucleosynthesis).

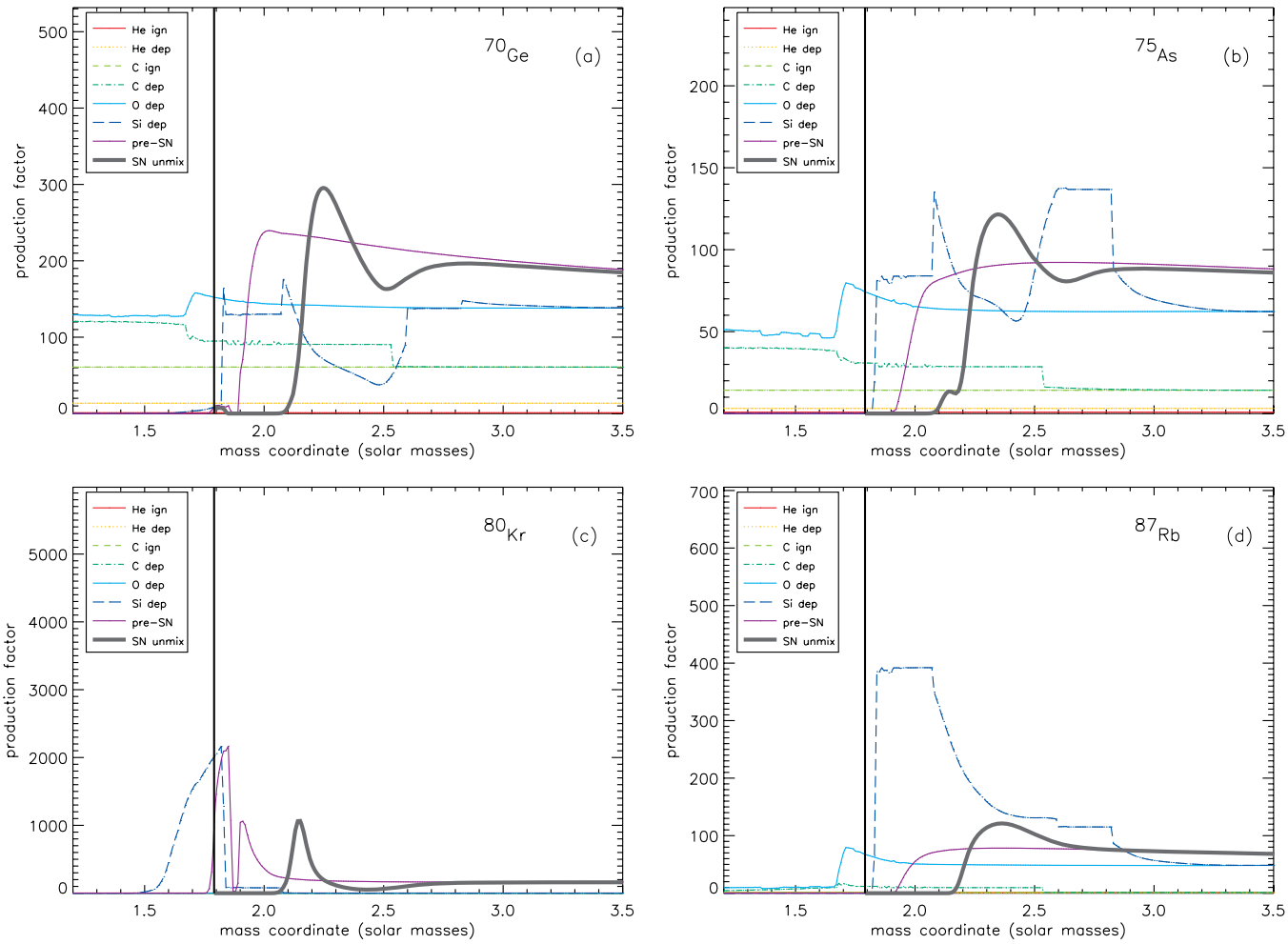

Figure 8. Production factor vs. the mass coordinate (1.2–3.5 $M_{\odot}$) for a 25 $M_{\odot}$ star viewed at various times during the star's life for (a) ^{70}Ge, (b) ^{75}As, (c) ^{80}Kr, and (d) ^{87}Rb. The figures are plotted for the central values of the helium burning reaction rates. The thick vertical line shows the location of the initial mass cut.

(A color version of this figure is available in the online journal.)

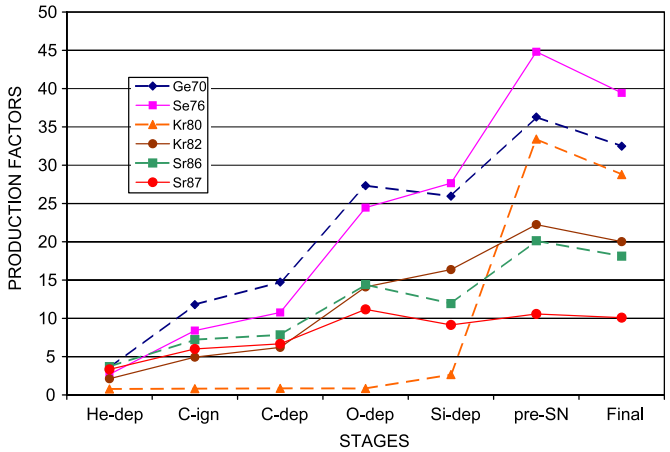

Figure 9. Production factors of *s*-only nuclei lying outside the mass cut at various evolutionary stages for a 25 $M_{\odot}$ star using the central values of the reaction rates and the L03 abundances.

(A color version of this figure is available in the online journal.)

the changes in the amount of carbon left at the end of central helium burning, and the amount of ^{22}Ne burnt in central helium burning.

In most cases, our simulations yield lower PFs for the abundances of L03 than for the abundances of AG89; the lower CNO content of the L03 abundance set is responsible for the reduced efficiency of the *s*-processing. This tendency is not always followed, however, as we see for the *s*-only nuclei with the central rates, in Table 2. The production of the weak-*s* nuclei is highly sensitive to the rates of the helium burning reactions. In some cases (see the discussion of the results of Table 2), we find that a 15% change in these rates may change the nucleosynthesis rates by more than a factor of 2.

Table 3
Fraction of Sr, Y, Zr Produced in the Weak *s*-Process—L03 Abundances

Element	PF-max	PF-min	*f*-max[a]	*f*-min[a]	Δf[b]
		25 $M_{\odot}$ star			
Sr	8.17	3.30	0.27	0.11	0.16
Y	5.76	2.64	0.19	0.09	0.10
Zr	5.24	2.09	0.17	0.07	0.10
		IMF average of 15 $M_{\odot}$, 20 $M_{\odot}$, and 25 $M_{\odot}$ stars			
Sr	4.402	2.201	0.144	0.072	0.072
Y	2.844	1.918	0.093	0.063	0.030
Zr	3.089	1.519	0.101	0.050	0.051

Notes.
[a] Calculated from Equation (1).
[b] *f*-max − *f*-min: spread of fractional production among calculated reaction rates.

We find that one must follow the entire evolution of the star to evaluate accurately the contribution of massive stars to *s*-process abundances. Most earlier studies took into account only the contribution of core He burning and shell C burning. We show that significant production takes place in later burning phases as detailed for the *s*-only isotopes in Figure 9. The burning phases beyond shell C burning mostly destroy isotopes in the core (especially near the mass cut), but overall lead to an increased production of some isotopes. The passage of the shock wave further modifies those PFs, usually reducing them slightly.

We have examined the uncertainties in the weak *s*-process production for Sr, Y, Zr owing to uncertainties in the helium burning reaction rates, and find that they are in the 3%–7% range. This is smaller than the observed deficiencies of 8%–18% in the known production mechanisms that led to the introduction of the LEPP process. On the other hand, we surely underestimate the total uncertainties. Uncertainties in the reaction rates of the neutron producing and capture reactions are significant. In addition, uncertainties in the stellar models can have significant effects (e.g., the treatment of hydrodynamics, convection, overshoot, etc.; see Costa et al. 2006 for a study of the effects of overshooting). We refer the reader to Tur et al. (2007) for a more complete discussion of those approximations and physics uncertainties. Combining all these uncertainties may render the evidence for the LEPP process less convincing.

We have shown that many aspects of nucleosynthesis in supernovae, the production of the medium-weight nuclei, as discussed in Tur et al. (2007), and that of the weak *s*-process nuclei described here, are highly sensitive to variations of the helium burning reaction rates, within their experimental uncertainties. This further emphasizes the need for better values of the helium burning reaction rates.

We thank Robert Hoffman for providing the solar-abundance sets used in this study and Stan Woosley for helpful discussions, including studies on the relative influence of the two reaction rates. This research was supported in part by the US National Science Foundation grants PHY06-06007 and PHY02-16783, the latter funding the Joint Institute for Nuclear Astrophysics (JINA), a National Science Foundation Physics Frontier Center. A. Heger performed his contribution under the auspices of the National Nuclear Security Administration of the US Department of Energy at Los Alamos National Laboratory under contract DE-AC52-06NA25396, and has been supported by the DOE Program for Scientific Discovery through Advanced Computing (SciDAC; DE-FC02-01ER41176).

REFERENCES

Anders, E., & Grevesse, N. 1989, Geochim. Cosmochim. Acta, 53, 197 (AG89)
Arnett, W. D., & Thielemann, F.-K. 1985, ApJ, 295, 589
Baraffe, I., El Eid, M. F., & Prantzos, N. 1992, A&AR, 258, 357
Buchmann, L. R. 1996, ApJ, 468, L127 (erratum ApJ, 479, L153 [1997])
Busso, M., & Gallino, R. 1985, A&AR, 151, 205
Caughlan, G. R., & Fowler, W. A. 1988, At. Data Nucl. Data Table, 40, 283
Costa, V., Pumo, M. L., Bonanno, A., & Zappala, R. A. 2006, A&A, 447, 641
Couch, R. G., Schmiedekamp, A. B., & Arnett, W. D. 1974, ApJ, 190, 95
Heil, M., Kaeppeler, F., Uberseder, E., Gallino, R., & Pignatari, M. 2008, Phys. Rev. C, 77, 015808
Hoffman, R. D., Woosley, S. E., & Weaver, T. A. 2001, ApJ, 549, 1085
Lamb, S. A., Howard, W. M., Truran, J. W., & Iben, I. 1977, ApJ, 217, 213
Langer, N., Arcoragi, J.-P., & Arnould, M. 1989, A&AR, 210, 187
Limongi, M., & Chieffi, A. 2003, ApJ, 592, 404
Lodders, K. 2003, ApJ, 591, 1220 (L03)
Montes, F., et al. 2007, ApJ, 671, 1685
Nassar, H., et al. 2005, Phys. Rev. Lett., 94, 092504
Prantzos, N., Hashimoto, M., & Nomoto, K. 1990a, A&AR, 234, 211
Prantzos, N., Hashimoto, M., Rayet, M., & Arnould, M. 1990b, A&AR, 238, 455
Raiteri, C. M., Busso, M., Gallino, R., & Picchio, G. 1991a, ApJ, 371, 665
Raiteri, C. M., Busso, M., Gallino, R., Picchio, G., & Pulone, L. 1991b, ApJ, 367, 228
Raiteri, C. M., Gallino, R., & Busso, M. 1992, ApJ, 387, 263
Raiteri, C. M., Gallino, R., Busso, M., Neuberger, D., & Kaeppeler, F. 1993, ApJ, 419, 207
Rauscher, T., Heger, A., Hoffman, R. D., & Woosley, S. E. 2002, ApJ, 576, 323
Rauscher, T., & Thielemann, F. K. 2000, At. Data Nucl. Data Tables, 75, 1
Scalo, J. M. 1986, Fundam. Cosm. Phys., 11, 1
The, L.-S., El Eid, M. F., & Meyer, B. S. 2000, ApJ, 533, 998
The, L.-S., El Eid, M. F., & Meyer, B. S. 2007, ApJ, 655, 1058
Travaglio, C., Gallino, R., Arnone, E., Cowan, J., Jordan, F., & Sneden, C. 2004, ApJ, 601, 864
Tur, C., Heger, A., & Austin, S. M. 2007, ApJ, 671, 821
Weaver, T. A., & Woosley, S. E. 1993, Phys. Rep., 227, 65
Weaver, T. A., Zimmerman, G. B., & Woosley, S. E. 1978, ApJ, 225, 1021
Woosley, S. E., & Heger, A. 2007, Phys. Rep., 442, 269
Woosley, S. E., Heger, A., Rauscher, T., & Hoffman, R. D. 2003, Nucl. Phys. A, 718, 3c
Woosley, S. E., Heger, A., & Weaver, T. A. 2002, Rev. Mod. Phys., 74, 1015
Woosley, S. E., & Weaver, T. A. 1995, ApJ, 101, 181